

SELF-GRAVITY AND ANGULAR MOMENTUM TRANSPORT IN EXTENDED GALACTIC DISKS

C.P. McNALLY^{1,2}, J. WADSLEY, AND H.M.P. COUCHMAN

Department of Physics & Astronomy, McMaster University, 1280 Main St. W, Hamilton, ON, L8S 4M1, Canada
Draft version November 19, 2018

ABSTRACT

We demonstrate a significant difference in the angular momentum transport properties of galactic disks between regions in which the interstellar medium is single phase or two phase. Our study is motivated by observations of H I in extended galactic disks which indicate velocity dispersions of non-thermal origin, suggesting that turbulence in the gas may be contributing significantly to the observed dispersion. To address this, we have implemented a shearing-box framework within the FLASH code. The new code was used to perform local simulations of galactic disks that incorporate differential rotation, self-gravity, vertical stratification, hydrodynamics and cooling. These simulations explore plausible mechanisms for driving turbulent motions via the thermal and self-gravitational instabilities coupling to differential rotation. Where a two-phase medium develops, gravitational angular momentum transporting stresses are much greater, creating a possible mechanism for transferring energy from galactic rotation to turbulence. In simulations where the disk conditions do not trigger the formation of a two-phase medium, it is found that perturbations to the flow damp without leading to a sustained mechanism for driving turbulence. The differing angular momentum transport properties of the single- and two-phase regimes of the disk suggest that a significant, dynamically motivated division can be drawn between the two, even when this division occurs far outside the star formation cutoff in a galactic disk.

Subject headings: hydrodynamics — galaxies: structure — gravitation

1. INTRODUCTION

The magnitude of the H I velocity dispersion in the outer regions of galactic disks is observed to be surprisingly consistent, about $7 \pm 1 \text{ km s}^{-1}$ (Santillán et al. 2007; particular examples are DDO 154, Dickey et al. 1990; ESO 215-G?009, Warren et al. 2004; and those discussed by Dib et al. 2006 and references therein). Though supernovae are accepted to be the main energy source for interstellar (ISM) turbulence where star formation occurs (see review by Mac Low & Klessen 2004) the driving mechanism for turbulence where this is not the case is unclear. Theoretical arguments have been made by Sellwood & Balbus (1999) and Piontek & Ostriker (2007) that this turbulence is magnetorotational instability (MRI) turbulence, and by Santillán et al. (2007) that it is driven through the infall of gas clouds.

Typically, the stellar disk does not stop immediately at a well-defined radius; most commonly the rate at which the brightness profile declines switches to a much steeper exponential than in the inner disk. This double exponential profile has been characterized by Pohlen et al. (2008). Theories predicting a sharp cutoff to star formation, such as the Q criteria of Kennicutt (1989) and the cold-phase criteria of Elmegreen & Parravano (1994) and Schaye (2004) do not naturally explain this profile. However, the theory of Elmegreen & Hunter (2006), which includes a second regime of turbulence-triggered star formation outside the cutoff radius, may produce such double exponential profiles. Additionally, Debattista et al.

(2006) suggest that an initial single-exponential brightness profile could evolve into a double-exponential one through secular effects.

Low-level star formation in the extended disk would require the cold phase to exist in at least some regions, indeed de Blok & Walter (2006) observed both a warm and a cold phase outside the observed limit of star formation in NGC 6822.

Self-gravity in conjunction with differential rotation has been examined as a mechanism for driving turbulence by Wada & Norman (1999, 2001, 2007) and Wada et al. (2002) with global two-dimensional and three-dimensional models of a galactic disk including self-gravity and cooling. In order to release energy with which to drive turbulence, self-gravitational interactions must lead to angular momentum transport. Hence it is important to analyze the criteria under which self-gravitational angular momentum transport can occur.

Following Lynden-Bell & Kalnajs (1972) and Sellwood & Balbus (1999) we introduce the mass-weighted average angular momentum transporting stress $\langle T_{xy} \rangle$. The xy subscript results from this being evaluated in a local set of Cartesian coordinates around one point in the disk. In this frame, x is the radial coordinate and y is the azimuthal coordinate. The gas perturbed velocity is denoted by \mathbf{u} and the gravitational velocity is defined as $\mathbf{u}_G \equiv \nabla\Phi/\sqrt{4\pi G\rho}$ following Sellwood & Balbus (1999). Then the xy component of the stress, which transports angular momentum, is

$$\langle T_{xy} \rangle \equiv \langle \rho u_x u_y + \rho u_{Gx} u_{Gy} \rangle. \quad (1)$$

The first term in this expression is the hydrodynamic stress, or T_{xy}^{hydro} , and the second is the gravitational stress, or T_{xy}^{grav} . The mass-weighted average values of these, $\langle T_{xy} \rangle$, will be used to detect whether a disk has

arXiv:0904.4251v1 [astro-ph.GA] 27 Apr 2009

Electronic address: colinm@astro.columbia.edu

Electronic address: wadsley@mcmaster.ca

Electronic address: couchman@mcmaster.ca

¹ Current address: Department of Astronomy, Columbia University, 550 West 120th Street, New York, NY, USA 10027

² Corresponding author

the ability to drive turbulence through the coupling of differential rotation to local motions.

Wada & Norman (2007) have performed global simulations of self-gravitationally driven turbulence in a galactic disk. In comparison to the initial conditions used in this work (see Section 3.1) the initial conditions of Wada & Norman (2007) lie far into the thermally unstable regime. Those simulations are not accompanied by a direct analysis of the role of angular momentum transport in driving the turbulence. This paper carefully examines the evolution of angular momentum transport. Piontek & Ostriker (2007) have performed local simulations of MRI in the context of a galactic disk with a two-phase medium, but do not examine self-gravity. In this paper, we present the results of simulations showing the difference in self-gravitational angular momentum transport properties of single-phase and two-phase galactic-type disks. We also demonstrate the onset of this mode of angular momentum transport when a single-phase accreting disk gains sufficient surface density to form a two-phase medium. This was done by a series of models of local disk patches, with either fixed mass or continuous accretion. The possible regimes of behavior for a local patch of galactic disk are then discussed.

2. METHODS

We began with the standard FLASH 2.3r1 code (Fryxell et al. 2000) which, among other features, included support for parallel adaptive mesh hydrodynamics and self-gravity in periodic boundary conditions. We implemented support for shearing-box boundary conditions and fictitious forces, shearing-box self-gravity, and modified the hydrodynamics for the shearing frame. The background shearing flow was split from the hydrodynamics, in a manner similar to Masset (2000) and Gammie (2001). The evolution of linear shearing waves has been tested, as in Johnson & Gammie (2005) and Shen et al. (2006).

To handle the combination of both self-gravity (Poisson’s equation) and the shearing frame (Hill’s equations; Hill, 1878) three choices are made. First, the vertical background force term, originally $\Omega^2 z$, was transitioned to 0 in the range $z_c < z < 2z_c$, where z_c is a parameter, by means of a cubic interpolation. The vertical external gravity was hence zero at the vertical boundaries. Second, the vertical fluid boundary is set to either zero-gradient (outflow) or a fixed-value (inflow). Third, self-gravity is solved with a periodic boundary condition in the vertical direction, and the simulation box kept tall and thin so that the combination of the self-gravity and the vertical background force produces a boundary condition essentially equivalent to an isolated boundary condition for the disk.

The shearing box is specified by two parameters, the angular frequency Ω and the radial rate of change of this quantity, $q \equiv -d \ln \Omega / d \ln R$. To simulate an outer galactic disk, these are chosen as $\Omega = 8.9 \times 10^{-16} \text{ s}^{-1}$ and $q = 1$.

As the shearing box is a local model, global self-gravitational phenomena such as spiral arms and bars cannot be captured. The shearing box also forces the angular momentum transport to be purely local, i.e. within the scale of the box (Balbus & Papaloizou 1999). In the context of this work, this is an advantage, as the mecha-

nisms produced will be local and minimal in nature, not relying on the large-scale structure of the galaxy, and hence are, perhaps, more generally applicable.

2.1. Cooling

We investigate the significant difference in behavior between single- and two-phase disks. The formation of a two-phase disk is dependent on the radiative cooling used. To include the local effects of various optically thin limit cooling and heating mechanisms a net heat loss function is defined as $\mathcal{L}(T) \equiv \rho \Lambda(T) - \Gamma$, where Γ is a constant following Brandenburg, Korpi, & Mee (2007) and others. We use a heating parameter $\Gamma = 0.015 \text{ erg g}^{-1} \text{ s}^{-1}$ as in Brandenburg et al. (2007) and Piontek & Ostriker (2007). The form of $\Lambda(T)$ is a piecewise power-law fit from Brandenburg et al. (2007). The resulting heating equilibrium curve is shown in Figure 1. For calculating temperature, the mean particle mass is $\mu = 0.62$ and a $\gamma = 5/3$ ideal gas equation of state is used. To ensure that the Jeans length is resolved, the Jeans length limiter is taken from Wada & Norman (2007). This is designed to prevent artificial fragmentation by enforcing a minimum value of the Jeans length (Truelove et al. 1997). The Jeans limiter artificially halts collapse where it can still be resolved without artificial fragmentation. Runs were stopped when the computational expense became prohibitive. Whether the collapse stops in real disks, and how, cannot be addressed by these models.

3. RESULTS

3.1. Fixed Mass Disk

The important parameter in fixed-mass disk models is where the phase of the mid-plane lies in relation to the critical curve for thermal instability. Disks in which the densest parts have perturbations that are sufficiently strong to trigger thermal instability, form a two-phase medium. Seven models with disks of fixed mass and cooling were run. The models had parameters such that the mid-plane conditions varied around the heating-cooling equilibrium curve on the ρ - P phase diagram. These models provided characterizations of the possible two-phase and single-phase disks. The parameters of these runs were a box $1.2 \text{ kpc} \times 1.2 \text{ kpc} \times 4.8 \text{ kpc}$, with no minimum level of refinement. The standard resolution run used four levels of refinement at the mid-plane or a mid-plane resolution of 128^2 and 9.375 pc . The initial condition was a hydrostatic equilibrium isothermal disk, with 1% random density perturbations added to each cell. Runs with surface density $\Sigma = 6 \text{ M}_\odot \text{ pc}^{-2}$ and initial temperature 2500 K , the standard mid-plane resolution, and double the standard resolution developed a two-phase medium. An additional variation with $\Sigma = 15 \text{ M}_\odot \text{ pc}^{-2}$ and initial temperature $10,000 \text{ K}$ also developed this two-phase medium. The unstable filaments connecting the lumps are gradually accreted into clouds and an unstable layer exists as a sheath around the cool clouds. A Q -stable disk of thermally stable gas remains extending far above the clouds. The phase diagram of this two-phase medium consists of points lying on the warm thermal equilibrium line, a scatter of points proceeding across to the cold equilibrium line below the peak warm equilibrium pressure, points lying on the cold equilibrium line, and a small

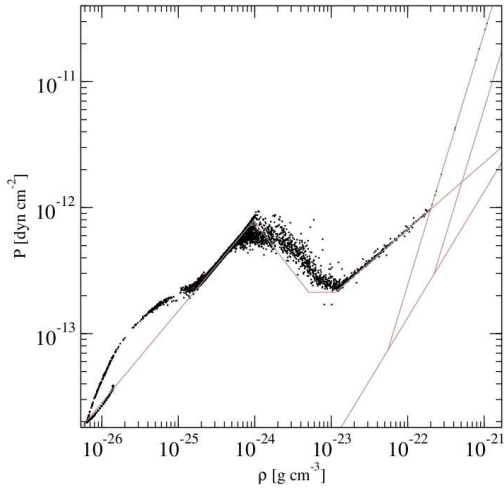


FIG. 1.— Run A1 gas phase distribution at $t = 2.73 \times 10^{16}$ s with equilibrium curve and temperature limits

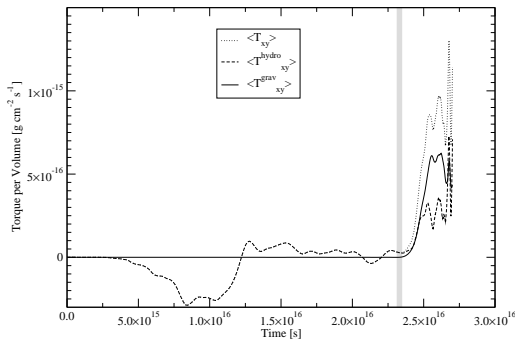


FIG. 2.— Run A1 stress – showing the transition from stable to unstable evolution as the cool phase develops, the gray vertical stripe marks the onset of the formation of the cool phase, the jump in $\langle T_{xy}^{\text{grav}} \rangle$ is approximately a factor of 10^4

number of points lying on the Jeans limiter line. This is similar to the phase diagram for the late time of the accreting disk shown in Figure 1. When the disk is single-phase, it evolves toward a smooth shearing flow without significant angular momentum transporting stress. The four remaining runs evolved to this state. Additionally, Toomre-stable isothermal gas disks (without cooling) also behaved in this manner.

Even in the two-phase disk runs, the total mass-weighted value of the Toomre Q parameter (Toomre 1964; Goldreich & Lynden-Bell 1965) stays well in the range of stability. For example, $Q > 4.5$ for all times in the first two-phase run described, even though the cool phase by itself is Toomre-unstable. The self-gravitational stresses of two-phase fixed mass disks are essentially the same as the two-phase part of the accreting disk to be discussed in Section 3.2.

3.2. Accreting Disk

Run A1 starts with the grid as in the standard resolution fixed-mass disk in the previous section, but with an initial condition of uniform very low den-

sity (10^{-28} g cm $^{-3}$) gas. Inflow z -direction boundaries were specified with the inflow rate set as 1.146×10^{-8} M_{\odot} pc $^{-2}$ yr. Along the 16×16 grid of cells at the z -boundary, the density is 1% greater on odd-numbered rows. This provides a minimal but nonangular momentum transporting perturbation to the flow, so that the imposed perturbations will be larger than those arising from purely numerical effects. With these boundary conditions, the disk built up and eventually reached the critical temperature/pressure for thermal instability and formed a cool phase. The inflow rate was chosen to be slow so that the cool phase formation is not triggered directly by the inflow pressure.

The disk starts at very low surface density and slowly builds. As the infalling gas from either boundary collides with the disk it drives turbulence in the disk as it builds. This is however purely a function of the inflow boundary conditions. As the disk surface density grows, so does the mid-plane pressure, until eventually it is sufficient to trigger thermal instability, and the cool phase readily forms. Turbulence driven by the infalling gas creates density perturbations which the formation of the cool phase amplifies. As these cool lumps form and rapidly accrete gas, the gravitational interactions between them lead to vastly increased angular momentum transporting gravitational stress, as shown in Figure 2. When the gravitational stress amplifies as a result of the phase transition the change is dramatic: in the case of run A1 it is 4 orders of magnitude. After the cool phase forms, the phase diagram is like that displayed in Figure 1. Gas is introduced at a point near the heating-cooling equilibrium, initially expands and cools as it falls in, then recompresses and heats, rising above the equilibrium line toward higher densities. There is then a layer of gas lying along the equilibrium line, until the critical pressure for the phase change is reached. A further scatter of points on the phase plot shows the layer of cells around the cool clouds where gas is unstable and cooling onto the clouds. Finally, points denoting the cool clouds are distributed along the cool equilibrium line.

The run A2 repeats the same setup as run A1, but with half the mass inflow rate. A2 has the same pattern of rapidly growing stresses, with the transition at approximately the same surface density, demonstrating the critical importance of surface density rather than sensitivity to the imposed inflow rate. Between runs A2 and A1 the pre-transition hydrodynamic stresses vary in a different manner, demonstrating that they are indeed a function of the imposed boundary conditions.

4. DISCUSSION AND CONCLUSIONS

Two primary conclusions can be drawn from this work. First, thermal instability can trigger self-gravitational angular momentum transport. Second, the development of the cool phase leads to rapidly growing local self-gravitational angular momentum transporting stress.

The thermally stable cooling disks of fixed mass decayed toward a smooth flow state. Similarly, before the onset of thermal instability, the accreting disk models did not have significant self-gravitational stress. However, the combined results of the fixed-mass disk with cooling and the accreting disk simulations show that thermal instability and the formation of a two-phase medium can provide a mechanism for producing enhanced angu-

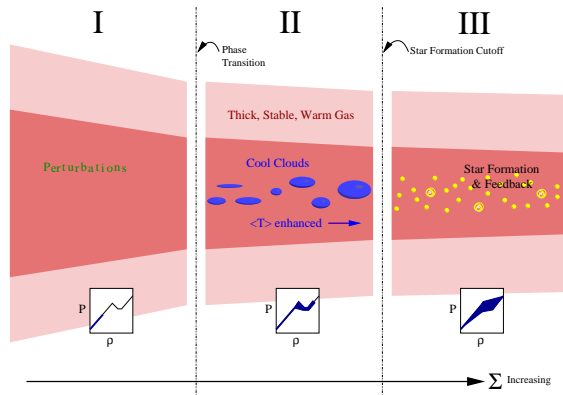


FIG. 3.— Three regimes of a galactic disk, the $P - \rho$ insets show which parts of the phase diagram are populated around the cooling-heating equilibrium curve

lar momentum transport by self-gravitational stresses. This will have two consequences: the galaxy’s rotational energy is converted into local motions giving rise to velocity dispersion in the gas; and it enhances the rate at which mass, primarily in the form of cool gas clouds, is transported inward enhancing the surface density of more central regions of the galactic disk. Increased surface density may in turn lead to star formation.

If the observed roughly constant velocity dispersion in the outer galactic disk is to be driven by a local self-gravitational mechanism, the simulations in this work suggest that the cool phase must exist everywhere in the disk where the velocity dispersion is seen. However, as the surface density of the disk drops, it will be increasingly difficult to achieve the critical pressure for the existence of the cool phase at the disk mid-plane. Detailed observations, extending the work of de Blok & Walter (2006), might settle this by directly detecting a cool phase in extended, low-surface-density galactic disks.

Finally, a picture of the phase structure and dynamic structure of the outer regions of a galactic disk can be drawn. Three regimes, as shown in Figure 3, can be identified, with the divisions between them drawn by the cutoff in star formation and the gas single-phase to two-phase transition.

- I A region of single phase gas, closely following the heating-cooling equilibrium curve on the phase diagram, with $Q > 1$, and with pressure too low to support a two-phase medium. Includes small perturbations. The total disk is Toomre-stable.
- II A region where pressure is sufficient for cool clouds to form from existing small perturbations, forming a two-phase medium, enhanced angular momentum transporting stresses result. The total disk is Toomre-stable.
- III The stellar disk, where the conditions for star formation are widely satisfied, and feedback (supernovae and outflows) drives turbulence. The total disk has Toomre Q satisfying a Kennicutt (1989) relation.

Regions I and II are simple to form - thick warm gas disks are physically simple, and the stellar disk is well known to exist. There are already a number of elements pointing to the nature of region II. Piontek & Ostriker

(2007) point out that the Schaye (2004) hypothesis, that the formation of the cool phase necessarily implies star formation, fails based on current observations showing that the phase change can occur outside the cutoff of star formation. That a region where turbulence must be driven by nonstellar processes while the cool phase exists has also been argued by Ostriker (2007). In the same work, they also find that magnetohydrodynamic effects in a region with cool clouds, such as in region II, may suppress star formation. The presence of star formation sets the division between regimes II and III. This cutoff may not be sharp and it could be expected that locally star formation may happen in the cool phase of region II. The presence of stars, and their feedback (particularly supernovae, see Mac Low & Klessen, 2004) changes the dynamics and phase structure of gas from II to III. Between regimes I and II the dividing line is drawn on the existence of the cool phase. In terms of the importance of local self-gravity in galactic disks, this work has shown that there is a significant energetic divide between regimes I and II.

The self-gravity and hydrodynamic stresses presented here in media with nonzero shear can be calculated and can be of similar magnitudes in nonshearing cases. A version of run A1 without shear was performed to demonstrate this. The definition of the stresses does not depend explicitly on the existence of nonzero shear. However, without shear, these stresses are not significant as they cannot extract energy from the background shear or transport angular momentum without a nonzero shear to couple to.

In regime II simulations in this work, the mass weighted average power per unit volume from self-gravitational stresses is typically on the order of 10^{-29} erg cm^{-3} s^{-1} , a significant energy input in such a context (Mac Low & Klessen 2004). We have also demonstrated that the presence of self-gravity leads to larger velocity fluctuations as follows. In a fixed-mass disk, we evolved a $\Sigma = 6 M_{\odot} \text{pc}^{-2}$ disk with an initial temperature of 1250 K until a two-phase medium had developed. At this time the mass weighted RMS velocity of gas below 1000 K was 1.3 km s^{-1} . This state was then used as input for two further simulations: one with the normal self-gravity, and the second with a fixed vertical gravity that was obtained by horizontally averaging the vertical self-gravity forces in the input state. When it became computationally infeasible to evolve the simulations further, the self-gravity case had a mass weighted RMS velocity of gas below 1000 K that had grown to 2.6 km s^{-1} and was climbing, while the same quantity in the fixed-gravity case had fallen to 0.8 km s^{-1} and was declining.

The extent to which extended H I disks have regions of type II must be determined by observations detecting or showing the absence of a cool component. One existing example is the observations by de Blok & Walter (2006) of NGC 6822, which suggest that part of this disk may be characterized as regime II. Even in the relatively small box used in Section 3.1, the mass weighted RMS velocity of gas below 1000 K is 2 km s^{-1} . This is in the same ballpark as the observed H I velocity dispersions.

The software used in this work was in part developed

by the DOE-supported ASE / Alliance Center for Astrophysical Thermonuclear Flashes at the University of Chicago. This work was made possible by the facilities of SHARCNET. C.P.M. was partially supported by NSF

CDI grant AST08-35734. H.M.P.C. acknowledges the support of NSERC and CIFAR. J.W. acknowledges the support of NSERC.

REFERENCES

- Balbus, S. A., & Papaloizou, J. C. B. 1999, *ApJ*, 521, 650
 Brandenburg, A., Korpi, M. J., & Mee, A. J. 2007, *ApJ*, 654, 945
 de Blok, W. J. G., & Walter, F. 2006, *AJ*, 131, 363
 Debattista, V. P., Mayer, L., Carollo, C. M., Moore, B., Wadsley, J., & Quinn, T. 2006, *ApJ*, 645, 209
 Dib, S., Bell, E., & Burkert, A. 2006, *ApJ*, 638, 797
 Dickey, J. M., Hanson, M. M., & Helou, G. 1990, *ApJ*, 352, 522
 Elmegreen, B. G., & Hunter, D. A. 2006, *ApJ*, 636, 712
 Elmegreen, B. G., & Parravano, A. 1994, *ApJ*, 435, L121+
 Fryxell, B., Olson, K., Ricker, P., Timmes, F. X., Zingale, M., Lamb, D. Q., MacNeice, P., Rosner, R., Truran, J. W., & Tufo, H. 2000, *ApJS*, 131, 273
 Gammie, C. F. 2001, *ApJ*, 553, 174
 Goldreich, P., & Lynden-Bell, D. 1965, *MNRAS*, 130, 125
 Hill, G. 1878, *Amer. J. Math.*, 1, 5
 Johnson, B. M., & Gammie, C. F. 2005, *ApJ*, 635, 149
 Kennicutt, R. C., Jr. 1989, *ApJ*, 344, 685
 Lynden-Bell, D., & Kalnajs, A. J. 1972, *MNRAS*, 157, 1
 Mac Low, M.-M., & Klessen, R. S. 2004, *Rev. Mod. Phys.*, 76, 125
 Masset, F. 2000, *A&AS*, 141, 165
 Ostriker, E. C. 2007, in *IAU Symp.*, Vol. 237, ed. B. G. Elmegreen & J. Palous (Cambridge: Cambridge Univ. Press), 70–75
 Piontek, R. A., & Ostriker, E. C. 2007, *ApJ*, 663, 183
 Pohlen, M., Erwin, P., Trujillo, I., & Beckman, J. E. 2008, in *Astronomical Society of the Pacific Conference Series*, Vol. 390, Pathways Through an Eclectic Universe, ed. J. H. Knapen, T. J. Mahoney, & A. Vazdekis, 247–
 Santillán, A., Sánchez-Salcedo, F. J., & Franco, J. 2007, *ApJ*, 662, L19
 Schaye, J. 2004, *ApJ*, 609, 667
 Sellwood, J. A., & Balbus, S. A. 1999, *ApJ*, 511, 660
 Shen, Y., Stone, J. M., & Gardiner, T. A. 2006, *ApJ*, 653, 513
 Toomre, A. 1964, *ApJ*, 139, 1217
 Truelove, J. K., Klein, R. I., McKee, C. F., Holliman, II, J. H., Howell, L. H., & Greenough, J. A. 1997, *ApJ*, 489, L179
 Wada, K., Meurer, G., & Norman, C. A. 2002, *ApJ*, 577, 197
 Wada, K., & Norman, C. A. 1999, *ApJ*, 516, L13
 —. 2001, *ApJ*, 547, 172
 —. 2007, *ApJ*, 660, 276
 Warren, B. E., Jerjen, H., & Koribalski, B. S. 2004, *AJ*, 128, 1152